# Tail Currents in the Myelinated Axon of *Xenopus laevis* Suggest a Two-Open-State Na Channel

Fredrik Elinder and Peter Århem
Nobel Institute for Neurophysiology, and Department of Neuroscience, Karolinska Institutet, S-171 77 Stockholm, Sweden

ABSTRACT Na tail currents in the myelinated axon of *Xenopus laevis* were measured at −70 mV after steps to −10 mV. The tail currents were biexponential, comprising a fast and a slow component. The time constant of the slow tail component, analyzed in the time window 0.35–0.50 ms, was independent of step duration, and had a value of 0.23 ms. The amplitude, extrapolated back to time 0, varied, however, with step duration. It reached a peak after 0.7 ms and inactivated relatively slowly (at 2.1 ms the absolute value was reduced by ~30%). The amplitude of the fast component, estimated by subtracting the amplitude of the slow component from the calculated total tail current amplitude, reached a peak (three times larger than that of the slow component) after 0.5 ms and inactivated relatively fast (at 2.1 ms it was reduced by ~65%). The results were explained by a novel Na channel model, comprising two open states bifurcating from a common closed state and with separate inactivating pathways. A voltage-regulated use of the two pathways explains a number of findings reported in the literature.

## INTRODUCTION

The Na channel is responsible for the induction of the action potential in most excitable cells. It is also the main target for several medical drugs and natural toxins. Although the Na channel kinetics has been studied extensively, there is still no consensus about a more detailed kinetic scheme. Such a detailed scheme is essential, not only for understanding the molecular function of the channels, but also for understanding the highly nonlinear effects of certain pharmacological compounds (e.g., Elinder and Århem, 1991).

The tail current is a good indicator of the open-state kinetics. A number of studies have shown that the Na current tails of several cell types are multiexponential and/or time-variant with respect to the activating test pulse duration (Frankenhaeuser and Hodgkin, 1957; Armstrong and Bezanilla, 1977; Goldman and Hahin, 1978; Sigworth, 1981; Dubois and Schneider, 1982; Gilly and Armstrong, 1984; Hahin, 1988). However, an explicit description of the time evolution of the different tail components has not been given. Such a description should be valuable for establishing a detailed kinetic scheme of the Na channel.

The aim of the present study is to give such a quantitative description. We analyzed the time evolution of different tail currents after a test step of varying duration in myelinated axons of *Xenopus laevis*. The analysis confirmed the multiexponential character of the tail current. By specifically analyzing the slow component, we could conclude that the results are explained by a Na channel model that includes two open states with separate activation pathways. This deviates from most other Na channel models proposed, which exclusively assume one open state (Hodgkin and Huxley, 1952; Frankenhaeuser and Huxley, 1964; Patlak, 1991; Vandenberg and Bezanilla, 1991). It also deviates from (the relatively few) other two-open-state models proposed in the literature (Chandler and Meves, 1970; Armstrong and Bezanilla, 1977; Sigworth, 1981; Ochs et al., 1981; Nagy, 1987; Keynes, 1994; Correa and Bezanilla, 1994). The presented model will be used to explain a number of findings reported in the literature.

## MATERIALS AND METHODS

### Voltage-clamp apparatus and procedures

Large myelinated axons were isolated from the sciatic nerve of unanesthetized decapitated toads of the species *Xenopus laevis*. Single axons were mounted in a recording chamber and cut at half-internode length on both sides of the node under investigation. Vaseline seals were used to separate the electrolyte pools. The chamber was connected by KCl bridges to the voltage-clamp apparatus. The chamber design, circuitry, and balancing, as well as calibration procedures, were essentially the same as described by Dodge and Frankenhaeuser (1958), with modifications to optimize the frequency response of the system, as described by Århem et al (1973). To obtain optimal feedback control and a favorable time resolution, all experiments were performed at low temperature (5°C).

The pulse protocol used is shown in Fig. 1. It consists of 1) a prepulse of 80 ms to −90 mV, 2) an intermediate pulse of 0.1 ms to −70 mV, 3) a test pulse of variable duration (0.1–2.9 ms in increments of 0.2 ms) to −10 mV, and 4) a postpulse to −70 mV. The prepulse was used to eliminate the steady-state inactivation, the intermediate pulse to reduce the induced capacitive current when changing the membrane potential to −10 mV. The holding potential was −70 mV. The leakage and remaining capacitive currents were eliminated from the test and postpulse-induced currents by subtracting currents generated by an inverted test pulse to −130 mV. The resulting tail currents showed some initial oscillatory behavior, most likely caused by the limited frequency response of the system, imposed by the phase lag properties of the preparation (see Dodge and Frankenhaeuser, 1958). For the quantitative analysis, the first 0.1 ms of the tail current was therefore excluded.

Computations based on the data of Frankenhaeuser and Moore (1963) and Frankenhaeuser and Huxley (1964) suggest that the tail current analyzed is carried almost exclusively by Na ions; at the end of the test pulse

*Received for publication 10 December 1996 and in final form 3 April 1997.*
Address reprint requests to Dr. Peter Århem, Nobel Institute for Neurophysiology, Karolinska Institutet, S-171 77 Stockholm, Sweden. Tel.: +46-8-728-69-03; Fax: +46-8-34-95-44; E-mail: peter.arhem@neuro.ki.se.

0006-3495/97/07/179/07 $2.00

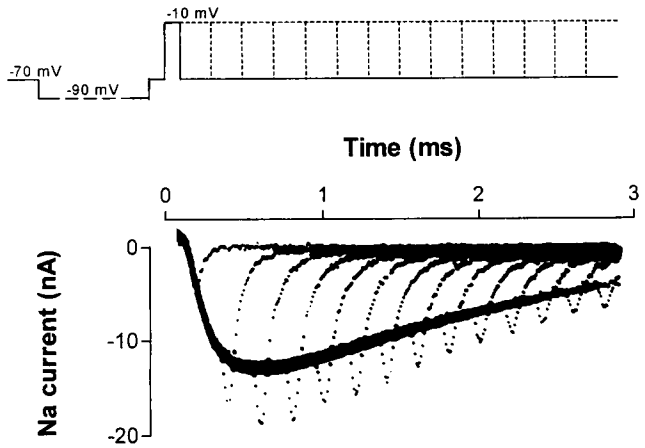


FIGURE 1 Na tail currents at −70 mV after a test step to −10 mV. The pulse protocol is shown in the upper panel. See text for detailed description. The first 50 μs of the recording is truncated.

(after 2.9 ms) the K current constitutes less than 4% of the total current and consequently less at earlier times.

The investigation was based on a relatively homogeneous population of axons. The variability of measured membrane parameters was low, indicated by the relatively small SD values. For six axons the mean time to Na current peak at −10 mV was 0.51 ± 0.07 ms, and the mean time to half-peak current during inactivation was 1.95 ± 0.24 ms.

## Solutions

The pool with the node under investigation contained Ringer's solution of the composition (in mM): NaCl 112, KCl 2.5, $CaCl_2$ 2.0, and Tris buffer (adjusted to pH 7.2) 2.5. The solution used in the end pools consisted of (in mM): KCl 120.0 and Tris buffer (pH 7.2) 2.5.

## Data acquisition and analysis

Pulse generation and acquisition of data were made by computer, utilizing an α16 (Computer Automation, Newport Beach, CA) and a 16-bit A/D converter (Teledyne Philbrick, Dedham, MA). The programs were written in assembler language. The results were displayed on an oscilloscope and recorded on photographic film.

## Computations

To quantitatively develop the model described in the text, we least-square-fitted the numerical solution of a system of parallel differential equations to experimental data. The model comprises three closed, two open, and two inactivated states, forming a slowly and a fast inactivating pathway. The probability $P_i$ that the channel is in state $i$ is described by the equation

$$dP_i(t)/dt = -\sum_{j=1}^{n} k_{ij}P_i(t) + \sum_{j=1}^{n} k_{ji}P_j(t),$$

$$i = 1, 2, \ldots, n; \quad j \neq i \quad (1)$$

where $n$ is the number of conformational states ($n = 7$ in the present case) and $k_{ij}$ is the transition rate from state $i$ to state $j$. To solve the equations, a simple Euler integration procedure was used. An integration step of 5 μs was found sufficient. At time 0 the channel was assumed to be in the most leftward state (see model). Initial values for the rate constants $k_{ij}$ were estimated from the experimental data (current at −10 mV). Because the time constant of activation ($\tau_m$ in the Hodgkin-Huxley nomenclature; 1952; Frankenhaeuser and Huxley, 1964) was roughly 0.1 ms, the initially guessed value of the rate constant for the first activation steps (a) was set to 10 $ms^{-1}$. Because the probability of opening in the fast inactivating pathway was ~0.8, the initially guessed value of the corresponding opening rate constant (b) was set to 8 $ms^{-1}$ (0.8 × 10 $ms^{-1}$), and consequently the initially guessed value for the opening rate constant of the slow pathway (d) was set to 2 $ms^{-1}$ (0.2 × 10 $ms^{-1}$). Because the time constant of inactivating the fast pathway was ~1 ms and that of the slow pathway was 4 ms, the initial values of the corresponding rate constants were set to 1 $ms^{-1}$ (c) and 0.25 $ms^{-1}$ (e). The fitting procedure consisted of a one-by-one step modification of the free parameters. When the fit did not improve for a change of the free parameters with 0.01%, the procedure was halted. The computations were made on a personal computer (CPU 80486), and the programs were written in BASIC.

## RESULTS

Fig. 1 shows typical Na tail currents after test pulses of increasing durations (pulse protocol shown in *top* of Fig. 1). Both amplitude and time course of the tails clearly depend on test pulse duration. The amplitude reaches a peak at a duration of ~0.5 ms, and the apparent rate of deactivation decreases with duration. The time course of each tail is complex. It shows a slight delay before reaching its peak, most likely depending on the limited frequency response of the system (see Materials and Methods). The phase after the peak is multiexponential. This is shown in better time resolution in Fig. 2 *A*, which shows the tail current after a 1.3-ms-long test pulse to −10 mV. The current values before 0.1 ms were distorted, as shown in Fig. 1 (see also Materials and Methods), and, beyond 0.5 ms, too small to be reliably measured and were therefore excluded in the figure.

### The time constant of the slow tail component

Fig. 2 *A* shows two single-exponential curves fitted by a least-squares procedure to two time segments of the tail current. One curve was fitted to the time segment 0.12–0.50 ms (*arrows 1 and 3*) and the other to the shorter time segment 0.35–0.50 ms (*arrows 2 and 3*). It is clear that only the fit to the shorter time segment is satisfactory. To determine the optimal time interval, we fitted exponentials to varying intervals with starting points between 0.12 and 0.45 ms. The resulting time constants increased (the amplitudes, extrapolated back to time 0, decreased) when the starting point increased from 0.12 to 0.35 ms, where a constant level was reached. Similar results were obtained for the relaxing component when we fitted the sum of one exponential and a constant (three variables), or for the slow component when we fitted a sum of two exponentials (four variables) to the data. In conclusion, the results suggest that the tail current contains a slow exponential component, which is possible to quantify by fitting a single-exponential curve to the current values in the time window 0.35–0.50 ms.

The time constant of the slow tail component was essentially independent of the duration of the test pulse. This is shown in Fig. 3, where the time constants of exponentials fitted to the optimal time window discussed above (0.35–

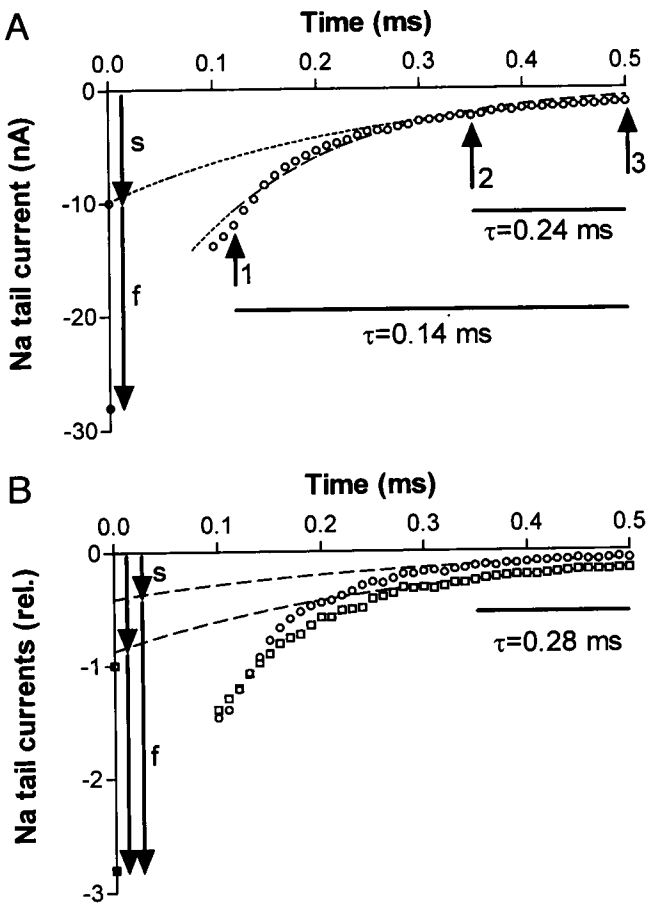


FIGURE 2 Estimating the components of the Na tail current at −70 mV after a test pulse to −10 mV. Data from Fig. 1. The first 0.1 ms are truncated. Arrows indicate the amplitude of the slow (s) and the fast (f) component extrapolated back to time 0. The unfilled symbols on the *y* axis indicate the amplitude at the end of the test pulse, and the filled symbols indicate the estimated instantaneous value at −70 mV (see text). (*A*) Single-exponential curves least-square fitted to the time segments 0.12–0.50 ms and 0.35–0.50 ms (*arrows*) of the tail current after a test pulse of 1.3 ms. Resulting time constants are indicated. (*B*) Single-exponential curves simultaneously fitted to the time segment 0.35–0.50 ms of the tail current after test pulses of 0.5 ms (*circles*) and 1.7 ms (*squares*). The currents are normalized to −1.0 at time 0. The amplitudes at time 0 are −0.41 and −0.87, respectively.

0.50 ms) after different test pulse durations are plotted. These results are in line with previous reports (Goldman and Hahin, 1978; Hahin, 1988). A small increase with duration (~25 μs/ms test pulse duration) was often seen but was not statistically significant. This increase could be due to a small steady-state component (as found in the three-variable fit above) or some residual fast component (as found in the four-variable fit above). Using the conclusion that the time constant of the slow tail component was independent of test pulse duration, we estimated the time constant by a simultaneous fit to all tails in one experiment. In Fig. 2 *B* a simultaneous fit to both curves (after 0.5 and 1.7 ms test pulse duration) in the time window 0.35–0.50 ms gave a common time constant of 0.28 ms. Fig. 4 shows the corresponding fit to 10 tails after test pulse durations from 0.3 to

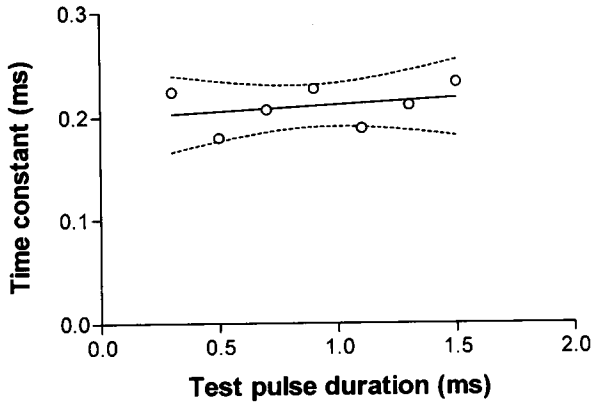


FIGURE 3 The time constant of the slow component of the tail current at −70 mV for varying durations of a test pulse to −10 mV. The estimations are based on fits to the time segment 0.35–0.50 ms. The continuous line is a linear least-square fit to the data points and has a slope of 13 μs/ms test pulse duration. The dashed lines indicate a 95% confidence interval.

2.1 ms. The resulting time constant was 0.24 ms. The mean (± SD) value for six axons was 0.23 ± 0.02 ms.

## The amplitudes of the two tail components

In Fig. 2 *A* the amplitude of the slow tail component, extrapolated back to time 0, is −10 nA. (Note that the coincidence between the current at the end of the test pulse at −10 mV and the extrapolated point does not imply a logical relationship.) To estimate the amplitude of the fast, experimentally unresolved component, we calculated the expected instantaneous value with the constant field equation (Dodge and Frankenhaeuser, 1959) and subtracted the slow tail component amplitude. The calculation of the instantaneous tail current yielded an increase in the current at the end of the test pulse with 180% if calculated for a Na

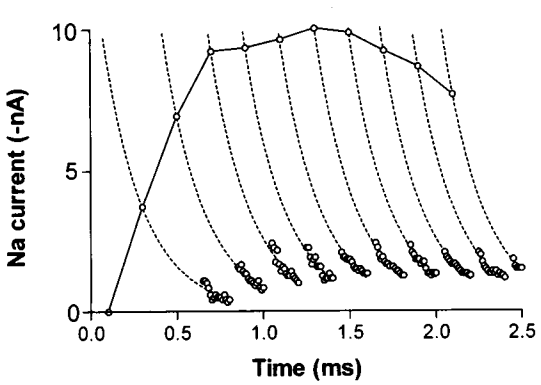


FIGURE 4 Time evolution of the slow tail component at −70 mV. Circles in clusters show the tail currents between 0.35 and 0.50 ms for 10 consecutive tails after a test pulse of varying duration (0.3–2.1 ms in steps of 0.2 ms) to −10 mV. Dashed lines are single-exponential curves simultaneously fitted to all data points shown. The resulting time constant is 0.24 ms. Circles connected with a continuous line show the amplitudes at time 0 for the fitted exponential curves.

equilibrium potential of +45 mV. It has been suggested that $Ca^{2+}$ instantaneously blocks the tail current, causing the instantaneous Na current to be smaller than predicted by the constant field equation (e.g., Armstrong and Cota, 1991). However, such an effect will not alter the main conclusions of the present paper. Assuming an increase at the end of the pulse with 100% instead of 180%, the estimations of the rate constants in the model developed below will maximally change with 20%. We consequently assumed that the tail currents were unblocked in the following analysis. In the case depicted in Fig. 2 *A*, the expected instantaneous current is −28 nA. Thus the slow component is about one-third of the expected total tail amplitude, leaving two-thirds for the fast component. In Fig. 2 *B* the relative amplitude (current at time 0 is set to −1) extrapolated back to time 0 is more than twice as large for the longer duration (*squares*) as for the shorter (*circles*). In Fig. 4 the time evolution of the slow component amplitude, extrapolated back to time 0, is displayed. As seen, the amplitude shows an initial, rapid increase, reaching a plateau of full amplitude after 0.7 ms, and a late, relatively slow inactivation.

Fig. 5 shows the time evolution of the mean amplitude of six axons (*open circles*) in comparison with the expected total tail current (*open squares*). The total current was calculated as the current at −10 mV multiplied by 2.8 (see above). The values for the total current from the different experiments were normalized to 1.0 at 0.5 ms, and the bars at the other time points indicate mean ± SEM. As seen, the peak (of the total current) is reached after 0.5 ms and the inactivation is relatively fast, the current reaching half-peak amplitude after 2.0 ms. The activation time course of the slow component (*open circles*) is almost as fast as that for the total current, and the peak is reached after 0.7 ms. However, the inactivation is much slower; the current is reduced by 30% at 2.1 ms. The difference between the amplitude of the total tail current and the slow component (*closed circles*) constitutes the amplitude of a fast tail component, the deactivation time course of which is unresolved. However, the time evolution of this component at −10 mV is given directly by the subtraction procedure and is shown in Fig. 5. As seen, the peak occurs after 0.5 ms and the inactivation is relatively fast, equaling the slow component at 2.5 ms.

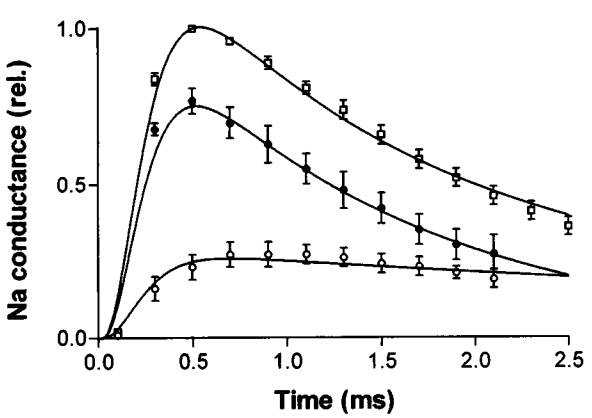


FIGURE 5 Amplitude of the tail current components at −70 mV versus test pulse duration. Open circles show the amplitude of the slow tail component at time 0 for each tail. Open squares show the corresponding total tail current, calculated as described in the text. Closed circles show the remaining fast component (*open squares* minus *open circles*). The total tail current at 0.5 ms is set to 1.0 in each experiment. Data are from six axons (mean ± SEM). The continuous lines are computed for the model described in the text. The open probability at the peak of total tail current is 0.79.

## Model fitting

Biexponential tail currents have repeatedly been reported before (see Introduction), and a number of explanatory models have been proposed. However, all explanations based on sequential single-open-state models can be shown to depend on either of two mechanisms (or combinations of them): 1) a two-step deactivation, in which the first transition is a fast equilibration and the second slow, or 2) a slow transition from an inactivated state and a fast transition to a closed. The two mechanisms are schematically described by the state diagrams below (activation transitions are from left to right, and deactivation as indicated by arrows in the opposite direction):

$$C_s \leftarrow C \underset{f_2}{\overset{f_1}{\leftrightarrow}} O \qquad \text{(Scheme 1)}$$

$$C_f \leftarrow O_s \leftarrow I \qquad \text{(Scheme 2)}$$

where C denotes closed, O open, and I inactivated states. The rate constants *f* and *s* indicate fast and slow transitions, respectively (at −70 mV). Both schemes give a biexponential deactivation. For Scheme 2 the time constants of the fast and the slow component are $1/f$ and $1/s$, respectively. For Scheme 1 the time constants are somewhat more complex to express; that of the fast component is approximately $1/(f_1 + f_2)$, and that of the slow component approximately $2/s$ (if $f_1 = f_2$). (The approximation depends on the size of the $f/s$ quotient; the larger the quotient, the better the approximation.) However, neither of the two schemes can explain the experimental results of the present investigation. The reasons are as follows: 1) Scheme 1 predicts that the slow tail component initially (when the intermediate C is substantially occupied) should be larger (if different) than the fast component. At later times (when both C states are unoccupied) the amplitudes of the two tail components should have the same time course. None of these predictions are fulfilled. 2) Scheme 2 predicts a delay in the build-up of the slow component with approximately the time course of the macroscopic inactivation. This was not seen in the experiments.

Obviously, an alternative to explain the observed tail currents is to assume different populations of Na channels, with different kinetics, or channels with different kinetic modes. However, there is experimental evidence for a homogeneous population of Na channels in the node of Ran-

vier (see Discussion). We therefore explored two open-state models. The following scheme, comprising two open states bifurcating from a closed state, was found to principally explain the observed tail currents:

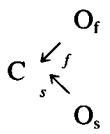


(Scheme 3)

This scheme was extended to a quantitative model to explain the experimental data on the activation and inactivation time courses shown in Fig. 5. The resulting model comprises three closed states (to account for the S-shaped activation) and two inactivated states, connected to the open states as shown below:

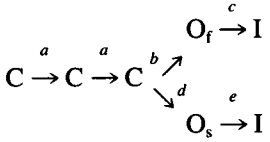


The transitions are assumed to be unidirectional at the discussed test pulse potential (−10 mV). This is justified by the fact that the experimentally determined peak current has reached maximum open probability at −10 mV (data not shown). The model further assumes equally conducting open states. As will be argued in the Discussion, this is supported by experimental evidence. The rate constants were determined by fitting currents predicted by the model to the mean current from six axons (see Fig. 5) by a least-squares procedure (see Materials and Methods). The resulting values were: $a = 13.0$, $b = 6.7$, $c = 0.72$, $d = 1.9$, and $e = 0.16\ ms^{-1}$. The computed time evolution of the two open states is shown in Fig. 5.

## DISCUSSION

In summary, the present investigation of the Na tail currents led us to develop a novel model for the Na channel in *Xenopus* axons, comprising two equally conducting open states bifurcating from a common closed state and with separate inactivating pathways. It was concluded that no single-open-state model can explain the experimental observations, nor can any multi-open-state model so far reported in the literature (see Introduction).

As mentioned above, the model was based on the assumptions that 1) the channel belongs to one homogeneous Na channel population and that 2) it does not switch between different gating modes (e.g., between slowly and fast inactivating modes). Both assumptions are supported by experimental studies. Thus there is no evidence for the existence of several Na channel populations in the amphibian node membrane (for a recent review, see Vogel and Schwarz, 1995). Single-channel studies (Jonas et al., 1989) have been unable to verify the two Na channel population hypothesis suggested by Benoit et al. (1985). Similarly, there is no evidence for the existence of different gating modes in nodal Na channels (Jonas et al., 1989). Recent studies (including single-channel recordings) of Na channel $\alpha$-subunits expressed in *Xenopus* oocytes suggest major gating mode shifts (Moorman et al., 1990; Zhou et al., 1991; Ji et al., 1994). This is reflected in, for instance, a clearly biphasic steady-state inactivation curve, not seen in the present case (Ji et al., 1994). However, for combined $\alpha$- and $\beta_1$-subunit Na channels, only one mode is observed (Ji et al., 1994). Studies of gating modes in native Na channels show only marginal shifts; for more than 99% of the time the channels are in the main mode (e.g., Patlak and Ortiz, 1986). Furthermore, detailed single-channel studies of a Na channel concluded to have several open states (sequentially arranged, in contrast to the bifurcating arrangement in the present model) suggest that the different open states belong to the same main mode (Nagy et al., 1983; Nagy, 1987).

Another assumption of the present model is equally conducting open states. (This assumption is in contrast to the two basic assumptions above not fundamental; assuming different conductance levels will only change the rate constants, but not the bifurcating scheme per se.) This assumption is supported by both fluctuation analysis and single-channel recordings of amphibian node Na channels (Sigworth, 1977; Jonas et al., 1989). Furthermore, for Na channels showing sublevel conductance states, the number of entries into the sublevel states are only ~1% of the number of main level state entries (Patlak, 1988).

### Implications of the model

In the present investigation the model was quantitatively developed only for −10 mV. However, making the assumptions that 1) the inactivation transitions are voltage independent (see, e.g., Aldrich et al., 1983; Cota and Armstrong, 1989) and 2) the $C \rightarrow O_f$ transition is more voltage dependent than the $C \rightarrow O_s$ transition, the model can explain a number of experimental findings reported in the literature:

1. It explains the voltage dependence as well as the biphasic shape of the inactivation time course in myelinated axons, with voltage-independent time constants and voltage-dependent amplitudes, the slow component being relatively larger at negative voltages and the fast component dominating at positive voltages (Chiu, 1977; Nonner, 1980; Sigworth, 1981; Ochs et al., 1981; Neumcke and Stämpfli, 1983; Benoit et al., 1985; Schmidtmayer, 1989; Jonas et al., 1989).

2. It explains the apparently non-Markovian behavior reported by Frankenhaeuser (1963), that during a voltage-clamp step to −10 mV the Na current initially inactivates more quickly when preceded by a short pulse to +30 mV than when not. The prepulse-induced inactivation time constant is equal to that associated with a pulse step to +30 mV. (Similar results have been reported for the squid axon by Chandler and Meves (1970).) In the present model the inactivation time course at −10 mV will be determined by

the properties of both the slow and the fast pathway. A positive prepulse will shunt most of the channels to the fast pathway, and the initial time course will consequently be determined by the kinetics of this pathway, independently of the magnitude of the test pulse. When the channels in the fast pathway have inactivated, the remaining inactivation time course will follow that caused by an unconditioned step to −10 mV, yielding the observed time course.

3. It explains the finding that the slowly inactivating component of the nodal Na channel dominates at negative potentials and activates at ~10 mV more negative potentials than the fast inactivating (peak) current. The two components have been shown to be about equal at −35 mV (Benoit et al., 1985). Making the quantitative assumptions that 1) the $C \rightarrow O_s$ transition is voltage independent and 2) the $C \rightarrow O_f$ transition depends exponentially on membrane voltage (see Stevens, 1978) with an *e*-fold change per 24 mV (derived from Frankenhaeuser, 1960), the model predicts equal amplitudes of the two components at −40 mV (the rate of the transition $C \rightarrow O_f$ equals that of $C \rightarrow O_s$). The two quantitative assumptions above also predict that the fast inactivating pathway will almost totally determine the macroscopic inactivation rate at positive potentials. At 20 mV the rate of $C \rightarrow O_f$ will be 12 times faster than that of $C \rightarrow O_s$. Thus the predicted value of the model will be close to 0.72 $ms^{-1}$ (rate constant *c* in the model). The largest value of the inactivation rate constant in the myelinated axon obtained experimentally (Frankenhaeuser and Huxley, 1964) is, after temperature correction (Frankenhaeuser and Moore, 1963), 0.9 $ms^{-1}$. The model also accounts for much of the observations that caused Gilly and Armstrong (1984) to postulate the existence of separate threshold channels, assumed to be important for the initiation of action potentials.

Furthermore, assuming that the two pathways are differently affected by different pharmacological compounds, the model can explain further experimental findings not well understood. For instance, a compound selectively blocking the $C \leftrightarrow O_f$ transition will reduce the peak current, increase the slow inactivating component, and make the tail current slower. Such an effect has been described for intracellularly applied tetramethylammonium (TMA) on squid axons (Yeh and Oxford, 1985).

### Temperature dependence

It is known that lowering the temperature reduces the peak Na current, while increasing the slowly inactivating current component in myelinated axons (Benoit et al., 1985; Schmidtmayer, 1989). This finding is accounted for by the present model, assuming a more temperature-sensitive opening of the fast pathway than that of the slow pathway. This, together with the proposals above of different voltage dependencies for the openings, suggests different molecular properties for the two transitions. The opening in the slow, voltage-independent pathway seems to be caused by some low-energy-barrier diffusion process, whereas the opening in the fast, voltage-dependent pathway seems to be directly associated with a high-energy-barrier transition in the voltage sensing system. Furthermore, assuming a selective temperature dependence like that discussed, the model predicts a channel behavior similar to that observed by Matteson and Armstrong (1982), which led them to postulate the existence of temperature-converted Na channels (sleepy channels).

## CONCLUDING REMARKS

In conclusion, our novel, bifurcating model explains the time evolution of the tail current components as well as hitherto unexplained properties of the Na channel inactivation and activation. The model implies a larger flexibility in responding to various effects than other models, a flexibility that accounts well for the highly nonlinear effects of pharmacological compounds on nervous activity at cellular as well as network levels. Recently, kinetic characteristics similar to those described here have been reported for L-type Ca channels (Fass and Levitan, 1996). The biexponential tail current of this channel was suggested to be generated by two open states, the slower component activating at more negative potentials than the fast component. This strengthens the view that voltage-gated Na and Ca channels are phylogenetically closely related (Hille, 1992). We conjecture that the two-open-state-induced kinetic complexity is a general characteristic of the action-potential-generating, four-domain Na and Ca channels, and that the phylogenetically more distant four-subunit K channels deviate from this pattern.

The experimental part of this investigation was done in collaboration with Bernhard Frankenhaeuser, who died in 1994.

Financial support from the Swedish Medical Research Council (project 6552), Karolinska Institutet, Swedish Society of Medicine, and Åke Wibergs Fonder is gratefully acknowledged.

## REFERENCES

Aldrich, R. W., D. P. Corey, and C. F. Stevens. 1983. A reinterpretation of mammalian sodium channel gating based on single channel recording. *Nature.* 306:436–441.

Århem, P., B. Frankenhaeuser, and L. E. Moore. 1973. Ionic currents at resting potential in nerve fibres from *Xenopus laevis*. Potential clamp experiments. *Acta Physiol. Scand.* 88:446–454.

Armstrong, C. M., and F. Bezanilla. 1977. Inactivation of the sodium channel. II. Gating current experiments. *J. Gen. Physiol.* 70:567–590.

Armstrong, C. M., and G. Cota. 1991. Calcium ion as a cofactor in Na channel gating. *Proc. Natl. Acad. Sci. USA.* 88:6528–6531.

Benoit, E., A. Corbier, and J.-M. Dubois. 1985. Evidence for two transient sodium currents in the frog node of Ranvier. *J. Physiol. (Lond.).* 361: 339–360.

Chandler, W. K., and H. Meves. 1970. Evidence for two types of sodium conductance in axons perfused with sodium fluoride solution. *J. Physiol. (Lond.)* 211:653–678.

Chiu, S. Y. 1977. Inactivation of sodium channels: second order kinetics in myelinated nerve. *J. Physiol. (Lond.).* 273:573–596.

Correa, A. M., and F. Bezanilla. 1994. Gating of the squid sodium channel at positive potentials. II. Single channels reveal two open states. *Biophys. J.* 66:1864–1878.

Cota, G., and C. M. Armstrong. 1989. Sodium channel gating in clonal pituitary cells. The inactivation step is not voltage dependent. *J. Gen. Physiol.* 94:213–232.

Dodge, F. A., and B. Frankenhaeuser. 1958. Membrane currents in isolated frog nerve fibre under voltage clamp conditions. *J. Physiol. (Lond.).* 143:76–90.

Dodge, F. A., and B. Frankenhaeuser. 1959. Sodium currents in the myelinated nerve fibre of *Xenopus laevis* investigated with the voltage clamp technique. *J. Physiol. (Lond.).* 148:188–200.

Dubois, J. M., and M. F. Schneider. 1982. Kinetics of intramembrane charge movement and sodium current in frog node of Ranvier. *J. Gen. Physiol.* 79:571–602.

Elinder, F., and P. Århem. 1991. Mechanisms of the tetrahydroaminoacridine effects on action potential and ion currents in myelinated axons. *Eur. J. Pharmacol.* 208:1–8.

Fass, D. M., and E. S. Levitan. 1996. L-type $Ca^{2+}$ channels access multiple open states to produce two components of Bay K 8644-dependent current in $GH_3$ cells. *J. Gen. Physiol.* 108:13–26.

Frankenhaeuser, B. 1960. Quantitative description of sodium currents in myelinated nerve fibres of *Xenopus laevis. J. Physiol. (Lond.).* 151: 491–501.

Frankenhaeuser, B. 1963. Inactivation of the sodium-carrying mechanism in myelinated nerve fibres of *Xenopus laevis. J. Physiol. (Lond.).* 169: 445–451.

Frankenhaeuser, B., and A. L. Hodgkin. 1957. The action of calcium on the electrical properties of squid axons. *J. Physiol. (Lond.).* 137:218–244.

Frankenhaeuser, B., and A. F. Huxley. 1964. The action potential in the myelinated nerve fibre of *Xenopus laevis* as computed on the basis of voltage clamp data. *J. Physiol. (Lond.).* 171:302–315.

Frankenhaeuser, B., and L. E. Moore. 1963. The effect of temperature on the sodium and potassium permeability changes in myelinated nerve fibres of *Xenopus laevis. J. Physiol. (Lond.).* 169:431–437.

Gilly, W. F., and C. M. Armstrong. 1984. Threshold channels: a novel type of sodium channel in the squid giant axon. *Nature.* 309:448–450.

Goldman, L., and R. Hahin. 1978. Initial conditions and the kinetics of the sodium conductance in *Myxicola* giant axons. II. Relaxation experiments. *J. Gen. Physiol.* 72:879–898.

Hahin, R. 1988. Removal of inactivation causes time-invariant sodium current decays. *J. Gen. Physiol.* 92:331–350.

Hille, B. 1992. Ionic Channels of Excitable Membranes. Sinauer Associates, Sunderland, MA.

Hodgkin, A. L., and A. F. Huxley. 1952. A quantitative description of membrane current and its application to conduction and excitation in nerve. *J. Physiol. (Lond.).* 117:500–544.

Ji, S., W. Sun, A. L. George, R. Horn, and R. L. Barchi. 1994. Voltage-dependent regulation of modal gating in the rat SkM1 sodium channel expressed in *Xenopus* oocytes. *J. Gen. Physiol.* 104:625–643.

Jonas, P., M. E. Bräu, M. Hermsteiner, and W. Vogel. 1989. Single-channel recording in myelinated nerve fibers reveals one type of Na channel but different K-channels. *Proc. Natl. Acad. Sci. USA.* 86: 7238–7242.

Keynes, R. D. 1994. The kinetics and voltage-gating of ion channels. *Q. Rev. Biophys.* 27:339–434.

Matteson, D. R., and C. M. Armstrong. 1982. Evidence for a population of sleepy channels in squid axon at low temperature. *J. Gen. Physiol.* 79:739–758.

Moorman, J. R., G. E. Kirsch, A. M. J. VanDongen, R. H. Joho, and A. M. Brown. 1990. Fast and slow gating of sodium channels encoded by single mRNA. *Neuron.* 4:243- 252.

Nagy, K. 1987. Evidence for multiple open states of sodium channels in neuroblastoma cells. *J. Membr. Biol.* 96:251–262.

Nagy, K., T. Kiss, and D. Hof. 1983. Single Na channels in mouse neuroblastoma cell membrane. *Pflügers Arch.* 399:302–308.

Neumcke, B., and R. Stämpfli. 1983. Alteration of the conductance of Na+ channels in the nodal membrane of frog nerve by holding potential and tetrodotoxin. *Biochim. Biophys. Acta.* 727:177–184.

Nonner, W. 1980. Relations between the inactivation of sodium channels and the immobilization of gating charge in frog myelinated nerve. *J. Physiol. (Lond.).* 299:573–603.

Ochs, G., B. Bromm, and J. R. Schwarz. 1981. A three-state model for inactivation of sodium permeability. *Biochim. Biophys. Acta.* 645: 243–252.

Patlak, J. B. 1988. Sodium channel subconductance levels measured with a new variance-mean analysis. *J. Gen. Physiol.* 92:413–430.

Patlak, J. B. 1991. Molecular kinetics of voltage-dependent $Na^+$ channels. *Physiol. Rev.* 71:1047–1080.

Patlak, J. B., and M. Ortiz. 1986. Two modes of gating during late Na+ channel currents in frog sartorius muscle. *J. Gen. Physiol.* 87:305–326.

Schmidtmayer, J. 1989. Voltage and temperature dependence of normal and chemically modified inactivation of sodium channels. *Pflügers Arch.* 414:273–281.

Sigworth, F. J. 1977. Sodium channels in nerve apparently have two conductance states. *Nature.* 270:265–267.

Sigworth, F. J. 1981. Covariance of nonstationary sodium current fluctuations at the node of Ranvier. *Biophys. J.* 34:111–333.

Stevens, C. F. 1978. Interactions between intrinsic membrane protein and electric field. *Biophys. J.* 22:295–306.

Vandenberg, C. A., and F. Bezanilla. 1991. A sodium channel gating model based on single channel, macroscopic ionic, and gating currents in the squid giant axon. *Biophys. J.* 60:1511–1533.

Vogel, W., and J. R. Schwarz. 1995. Voltage-clamp studies in axons: macroscopic and single-channel currents. *In* The Axon. S. G. Waxman, J. D. Kocsis, and P. K. Stys, editors. 257–280.

Yeh, J. Z., and G. S. Oxford. 1985. Interactions of monovalent cations with sodium channels in squid axons. *J. Gen. Physiol.* 85:603–620.

Zhou, J., J. F. Potts, J. S. Trimmer, W. S. Agnew, and F. J. Sigworth. 1991. Multiple gating and the effect of modulating factors on the μI sodium channel. *Neuron.* 7:775–785.